Forestry Research

ARTICLE

Open Access

https://doi.org/10.48130/forres-0026-0031

Forestry Research **2026**, 6: e032

MaDTX19 phosphorylation governs growth-defense trade-off under aluminum stress in mulberry

Shengmei Han[1#], Teng Zhao[1#], Chaorui Liu[1], Ming Sun[1], Jiaqi Zhao[2], Yuqi Wang[2], Zhaoyang Liu[1], Yingping Gai[2*] and Xianling Ji[1*]

[1] *College of Forestry, Shandong Agricultural University, Tai'an, Shandong 271018, China*
[2] *College of Life Sciences, Shandong Agricultural University, Tai'an, Shandong 271018, China*
[#] Authors contributed equally: Shengmei Han, Teng Zhao
[*] Correspondence: gyp@sdau.edu.cn (Gai Y); xlji@sdau.edu.cn (Ji X)

Abstract

The growth-defense trade-off is essential for plant adaptation to abiotic stress, yet the post-translational mechanisms underlying its dynamic regulation remain unclear. Here, we show that phosphorylation of the MATE transporter MaDTX19 at serine 4 (Ser4) acts as a critical regulatory node governing this trade-off in mulberry under Al^{3+} stress. *MaDTX19* expression was strongly upregulated by Al^{3+} stress, and its encoded protein underwent concurrent phosphorylation at Ser4. The phosphomimetic MaDTX19^{SD} mutant, but not the phosphodeficient MaDTX19^{SA} mutant, exhibited both growth inhibition and Al^{3+} tolerance, indicating that Ser4 phosphorylation is essential for these functions. Mechanistically, Ser4 phosphorylation enhanced the interaction of MaDTX19 with auxin-related proteins (Ma5NG4, MaWAT1, and MaAECC8), disrupting auxin homeostasis and suppressing growth. Concurrently, phosphorylated MaDTX19 promoted root citrate secretion and flavonoid accumulation while enhancing antioxidant enzyme activities, thereby conferring Al^{3+} tolerance through coordinated extracellular chelation and intracellular ROS scavenging. We further identified a MaMYB61-MaMYB308 transcriptional module in which MaMYB61 activates *MaDTX19* transcription through direct promoter binding, whereas MaMYB308 attenuates this activation by protein-protein interaction, allowing dynamic fine-tuning of *MaDTX19* expression to limit excessive fitness costs. Our study uncovers a phosphorylation-dependent mechanism by which a single MATE transporter coordinates growth-defense balance in a woody perennial, providing a genetic target for breeding Al^{3+}-tolerant mulberry cultivars on acidic marginal lands.

Keywords: Mulberry, MaDTX19, Aluminum stress, Phosphorylation, Growth-defense trade-off

Citation: Han S, Zhao T, Liu C, Sun M, Zhao J, et al. 2026. MaDTX19 phosphorylation governs growth-defense trade-off under aluminum stress in mulberry. *Forestry Research* 6: e032 https://doi.org/10.48130/forres-0026-0031

Introduction

Plants must constantly balance growth with defense against environmental stresses. This growth-defense trade-off is essential for optimizing resource allocation and ensuring fitness under adverse conditions[1,2]. Acidic soils occupy a large proportion of global agricultural land, where aluminum (Al^{3+}) toxicity represents a major factor limiting crop production. When soil pH drops below 5.0, soluble Al^{3+} rapidly inhibits root elongation and severely impairs water and nutrient uptake, posing a serious threat to global agricultural output and food security[3,4]. To counteract Al^{3+} toxicity, plants have evolved multiple defense mechanisms, among which MATE (Multidrug and Toxic Compound Extrusion) transporters play pivotal roles[5–7]. MATE proteins are characterized by 12 transmembrane domains and mediate the efflux of diverse substrates, thereby modulating plant development and stress adaptation[8–15]. A well-characterized mechanism of MATE-mediated Al^{3+} detoxification is the facilitation of root citrate secretion, which chelates toxic Al^{3+} in the rhizosphere[16,17]. Beyond organic acid efflux, certain MATE transporters participate in the vacuolar sequestration of flavonoids, including anthocyanins and proanthocyanidins[18–20]. These compounds can scavenge reactive oxygen species (ROS) under Al^{3+} stress, enhancing cellular redox homeostasis[21]. Additionally, some MATE members transport plant hormones such as auxin, directly linking them to growth and stress signaling pathways[22,23].

The interplay between auxin signaling and Al^{3+} tolerance pathways is particularly intriguing. As a key growth regulator, auxin modulates Al^{3+} tolerance through polar transport and cellular distribution[24–26]. Conversely, Al^{3+} stress disrupts auxin homeostasis. Notably, auxin signaling directly regulates Al^{3+}-responsive genes, including *MATE* genes, which in turn modulate auxin transport and accumulation[23,27–30]. This functional versatility positions MATE transporters as potential hubs balancing growth and stress responses. However, whether and how a single MATE protein directly coordinates this critical trade-off remains unclear. For instance, overexpression of *BoMATE* enhances Al^{3+} tolerance but reduces plant biomass[31], whereas *AtDTX50* improves drought tolerance without a growth penalty[32]. These findings highlight the context-dependent and functional diversity of the MATE family.

Current research has focused largely on transcriptional regulation of *MATE* genes, yet the potential for post-translational modifications to dynamically control MATE function has been largely overlooked. This is particularly important because plants facing acute Al^{3+} stress require immediate responses. Reversible phosphorylation offers a distinct advantage over transcriptional control by modulating protein activity within minutes, bypassing the time-consuming processes of transcription and translation[33–36]. Such a mechanism would enable rapid activation of detoxification and growth curtailment upon stress perception. However, whether post-translational modifications coordinate growth-defense trade-offs through a single MATE transporter in perennial woody plants remains unknown.

Precise transcriptional control of *MATE* genes is equally critical for optimizing the growth-defense balance. Constitutive or excessive

© The Author(s)

https://doi.org/10.48130/forres-0026-0031

expression of a growth-suppressing MATE transporter would impose continuous fitness costs even without stress. A finely tuned expression level, achieved through an activator-repressor transcriptional module, can ensure sufficient transporter activity during stress while preventing excessive fitness costs. Thus, the integration of rapid post-translational switches with precise transcriptional fine-tuning likely represents an evolutionarily optimized strategy for balancing immediate stress responses with long-term fitness.

Mulberry (*Morus alba*) is an economically important woody plant that exhibits exceptional resilience to environmental stresses, including extreme soil acidity (pH < 4.5)[37,38]. This inherent tolerance makes it an important plant for utilizing marginal land and an ideal model for deciphering sophisticated Al^{3+} tolerance mechanisms. Here, we identified an Al^{3+}-induced MATE gene, *MaDTX19*, from mulberry, and hypothesized that it acts as a central regulator integrating Al^{3+} stress and growth signaling, with activity controlled by a post-translational switch. Our objectives were to characterize the role of *MaDTX19* in regulating plant growth and Al^{3+} tolerance, validate the function of Ser4 phosphorylation in modulating MaDTX19 activity and protein-protein interactions, and elucidate the upstream transcriptional regulators and downstream pathways underlying its role in the growth-defense trade-off. Collectively, our findings reveal a phosphorylation-dependent mechanism by which a single MATE transporter coordinates growth-defense balance in a woody perennial, providing a genetic target for breeding Al^{3+}-tolerant mulberry cultivars on acidic marginal lands.

Materials and methods

Plant materials

Seedlings of mulberry ('Guisang you62', *M. atropurpurea*), *Arabidopsis thaliana* (Col-0 ecotype), and *Nicotiana benthamiana* were cultivated in growth chambers. Mulberry and tobacco were cultured at 26 °C with 50%–60% relative humidity under a 16 h light/8 h dark photoperiod. *Arabidopsis* was grown at 22 °C under the same humidity and photoperiod.

Phylogenetic and motif analysis

MATE family protein sequences from *A. thaliana* and *M. notabilis* were retrieved from NCBI. Multiple sequence alignment was performed using ClustalW in MEGA 6, and a neighbor-joining phylogenetic tree was constructed with 1,000 bootstrap replicates. Conserved motifs were identified using MEME (http://meme.nbcr.net/meme/intro.html) with default parameters. Transmembrane domains of MaDTX19 were predicted using TMHMM Server v.2.0.

Gene cloning and *Arabidopsis* transformation

Total RNA was extracted from mulberry leaves with TRIzol™ reagents (Invitrogen, Carlsbad, CA, USA) and reverse-transcribed using oligo (dT) primers (Invitrogen) and M-MLV Reverse Transcriptase (Promega, Madison, WI, USA). Target genes were amplified and cloned into plant expression vectors, and the resulting constructs were then transformed into *Agrobacterium tumefaciens* GV3101. *Arabidopsis* transformation was performed using the floral dip method. Transgenic lines were selected on 1/2 MS medium containing 50 mg·L^{-1} kanamycin and verified by PCR. Homozygous T_3 lines were used for subsequent experiments.

Generation of transgenic hairy roots

Target genes were inserted into the binary vector PLGNL under the control of the CaMV35S promoter and individually introduced into *A. rhizogenes* strain K599. Two-week-old seedlings of 'Guisang You 62' were wounded at the stem and infected with *A. rhizogenes* K599 harboring the target genes or an empty vector. Infected seedlings were co-cultured on MS medium in the dark for 2 d. Subsequently, they were transferred to selective MS medium supplemented with 50 mg·L^{-1} kanamycin and 100 mg·L^{-1} terramycin. Transgenic hairy roots emerged approximately four weeks later and were verified by PCR.

Subcellular localization analysis of MaDTX19

The coding sequence (CDS) of *MaDTX19* (without stop codon) was fused to *GFP* in the pCAMBIA1300 vector to construct 35S::MaDTX19-GFP. The recombinant vector and empty vector were transformed into *A. tumefaciens* GV3101 and infiltrated into *N. benthamiana* leaves. GFP fluorescence was observed 24–72 h post-infiltration under a Zeiss LSM880 laser scanning confocal microscope (Zeiss, Germany) (excitation/emission: 488/505–530 nm; chloroplast autofluorescence: 650 nm).

RT-qPCR

Total RNA was extracted as described above. RT-qPCR assays were performed using SYBR Premix Ex Taq II (TaKaRa Bio, Dalian, China) on a Bio-Rad CFX96™ System according to the manufacturer's protocols. *EF1-a* and *ACTIN* served as reference genes, and relative expression was calculated using the $2^{-\Delta\Delta C_T}$ method. Three independent biological replicates, each with three technical replicates, were analyzed per sample.

Promoter activity analysis

The *MaDTX19* promoter (*pMaDTX19*, a 2,000-bp fragment upstream of the start codon) was amplified from mulberry genomic DNA and fused to the β-glucuronidase (GUS) reporter gene in pBI121. One-week-old transgenic *Arabidopsis* seedlings carrying pMaDTX19::GUS were transferred to 1/2 MS medium supplemented with 50 μmol·L^{-1} ABA, 50 μmol·L^{-1} IAA, or 0.8 mmol·L^{-1} $AlCl_3$. Seedlings on normal medium served as controls. GUS staining was performed following the standard protocol[39], and stained tissues were photographed.

Aluminum stress treatment and determination of Al^{3+} content

Surface-sterilized *Arabidopsis* seeds were sown on 1/2 MS solid medium containing 0, 0.4, 0.8, or 1.2 mmol·L^{-1} $AlCl_3$. After stratification at 4 °C for 3 d, plates were transferred to growth chambers. Germination rates were scored daily, and root lengths were measured 7–10 d after germination. For physiological assays, four-week-old soil-grown *Arabidopsis* and mulberry seedlings were treated with 80 mmol·L^{-1} $AlCl_3$ solution, with water treatment as a control. The $AlCl_3$ concentrations were selected based on preliminary experiments and previous studies[40].

Al^{3+} accumulation in roots was visualized by hematoxylin staining. Roots were rinsed with distilled water and then stained with a freshly prepared solution containing 0.1% hematoxylin and 0.01% KI for 30 min. After thorough washing with distilled water, roots were photographed under a microscope.

For Al^{3+} content determination, plant samples were dried at 70 °C to constant weight, digested in 5% HNO_3 at 120 °C for 2 h, and

Al^{3+} concentration was measured by inductively coupled plasma mass spectrometry (ICP-MS; Agilent 7700x, USA).

Determination of physiological and biochemical parameters

Malondialdehyde (MDA) and proline contents were determined using assay kits (both from Solarbio, Beijing, China) according to the manufacturer's instructions. Citric acid content was assayed using a Citric Acid (CA) Content Assay Kit (Boxbio, Beijing, China). Anthocyanin was extracted with acidified methanol (1% HCl, v/v) and quantified by spectrophotometry[41], with three biological replicates per sample.

4-(Dimethylamino)cinnamaldehyde (DMACA) staining for proanthocyanidins

Samples were immersed in DMACA solution (containing 1% DMACA, 10% HCl, and 50% methanol) for 5–10 min. After staining, samples were rinsed with 70% ethanol and observed under a microscope. Magenta staining indicated proanthocyanidin accumulation.

Reactive oxygen species (ROS) detection and antioxidant enzyme activity assay

Histochemical staining for H_2O_2 and $O_2^{\cdot-}$ was performed with 3,3'-diaminobenzidine (DAB) and nitrotetrazolium blue chloride (NBT), respectively, using a Plant Tissue ROS Detection Kit (Solarbio, Beijing, China). Stained leaves were decolorized with 95% ethanol and photographed. Activities of superoxide dismutase (SOD), catalase (CAT), and peroxidase (POD) were determined with commercial assay kits (Solarbio, Beijing, China) following the manufacturer's methods.

Chlorophyll fluorescence imaging

Maximum photochemical efficiency of photosystem II (Fv/Fm) was measured with an IMAGING-PAM M-Series chlorophyll fluorescence system (Walz, Germany) after 30 min of dark adaptation. The minimal fluorescence (Fo) was measured under weak measuring light, and the maximal fluorescence (Fm) was determined after a saturating pulse of light. Fv/Fm was calculated as (Fm – Fo)/Fm.

Yeast one-hybrid assay (Y1H)

The *pMaDTX19* fragment was cloned into the pAbAi vector to generate pAbAi-pMaDTX19. Then, linearized pAbAi-pMaDTX19 plasmids were integrated into Y1HGold yeast to create bait-reporter yeast strains. The coding sequence of *MaMYB61* was cloned into pGADT7 to produce AD-MaMYB61. The plasmid AD-MaMYB61 was transformed into the bait yeast competent cells, and transformants were spread onto SD/-Leu/AbA selection medium and cultured at 28 °C for 3–5 d.

Luciferase reporter assay (LUC)

pMaDTX19 was cloned into the pGreenII 0800 vector, driving *LUC* expression. The CDSs of *MaMYB61* and *MaMYB308* were cloned into the pGreen62-SK effector vector, respectively, under the 35S promoter. Combinations of reporter and effector plasmids were transformed into *A. tumefaciens* GV3101 and co-infiltrated into *N. benthamiana* leaves. Luminescence was observed using a CCD (Charge-Coupled Device) camera 24–72 h later. Relative LUC activity was measured using a Dual-Luciferase Reporter Assay Kit (TransGen Biotech, China) and calculated as the ratio of firefly LUC to Renilla luciferase (REN).

Electrophoretic mobility shift assay (EMSA)

Recombinant MaMYB61 protein was expressed in *E. coli* BL21 and purified using Ni-NTA affinity chromatography. Biotin-labeled probes containing the predicted MaMYB61-binding site in the *MaDTX19* promoter were synthesized. Binding reactions were performed with purified protein and labeled probes, with unlabeled probes as competitors. Complexes were resolved on native polyacrylamide gels, transferred to nylon membranes, and detected using a chemiluminescent EMSA kit (Beyotime, China).

Membrane yeast two-hybrid assay

MaDTX19 was cloned into the pBT3-STE (bait) to generate the recombinant plasmid (pBT3- MaDTX19), and the CDSs of *MaAECC8*, *Ma5NG4,* and *MaWAT1* were cloned into pPR3-N (prey) to generate pPR3-MaAECC8, pPR3-Ma5NG4, and pPR3-MaWAT1, respectively. Bait and prey plasmids were co-transformed into yeast strain NMY51. The transformed cells were selected on SD/-Leu/-Trp (DDO) medium and tested for interaction on SD/-Ade/-His/-Leu/-Trp (QDO) medium. Yeast growth on QDO medium indicates a positive interaction.

Bimolecular fluorescence complementation assay (BiFC)

The CDS of *MaDTX19* was fused to the C-terminal half of YFP (YFP^C) in pSPYCE to generate a recombinant plasmid (MaDTX19-YFP^C). The CDSs of *MaAECC8*, *Ma5NG4*, and *MaWAT1* were fused to the N-terminal half (YFP^N) in pSPYNE, respectively, to generate MaAECC8-YFP^N, Ma5NG4-YFP^N, and MaWAT1-YFP^N. The *Agrobacterium* strain harboring the MaDTX19-YFP^C plasmid was mixed with strains containing MaAECC8-YFP^N, Ma5NG4-YFP^N, or MaWAT1-YFP^N plasmids, respectively. Mixtures were infiltrated into *N. benthamiana* leaves, and YFP fluorescence was detected 24–72 h post-infiltration using a Zeiss LSM880 confocal microscope (Zeiss, Germany) with excitation at 514 nm and emission collected at 520–560 nm.

Luciferase complementation assay (LCA)

The CDSs of *MaDTX19*, *MaDTX19^{SD}* (Ser4→Asp), and *MaDTX19^{SA}* (Ser4→Ala) were cloned into the pCAMBIA1300-nLUC (N-terminal LUC), respectively. The CDSs of *MaAECC8*, *Ma5NG4*, and *MaWAT1* were cloned into the pCAMBIA1300-cLUC (C-terminal LUC), respectively. *Agrobacterium* strains harboring nLUC and cLUC constructs were paired and infiltrated into *N. benthamiana* leaves. After 48–72 h, the leaves were sprayed with 1 mmol·L^{-1} luciferin and incubated in the dark for 5–10 min. Luminescence was captured using a CCD camera.

Western blot analysis

Total protein was extracted from root tips of *MaDTX19*-OE *Arabidopsis* treated with 0.8 mmol·L^{-1} $AlCl_3$ for various time points. Proteins were separated by SDS-PAGE and transferred to a PVDF membrane. For phosphorylation detection, the membrane was immunoblotted with a custom-made Anti-Phospho-(Ser/Thr) antibody (Abcam). For protein stability, total protein was extracted from *Arabidopsis* lines overexpressing *MaDTX19-GFP*, *MaDTX19^{SA}-GFP*, or *MaDTX19^{SD}-GFP* under Al^{3+} stress. Western blot was performed using an anti-GFP antibody (Abcam), and signals were visualized using chemiluminescence.

https://doi.org/10.48130/forres-0026-0031

Auxin content and distribution analysis

The auxin-responsive reporter DR5::GFP was transformed into WT and *MaDTX19*-OE *Arabidopsis*. Seedlings were treated with 0 or 0.4 mmol·L^{-1} $AlCl_3$ for 24 h, and GFP signals in root tips were examined under a confocal microscope. For auxin quantification, root tips were excised, and IAA content was quantified using an IAA ELISA Kit (Hengyuan Technology, China) according to the manufacturer's instructions.

Exogenous IAA treatment

For seedling assays, surface-sterilized WT and *MaDTX19*-OE *Arabidopsis* seeds were sown on half-strength MS medium supplemented with 0.5 μmol·L^{-1} IAA (dissolved in DMSO). Control seedlings were grown on medium containing equivalent DMSO. Plates were placed vertically under standard light conditions (16 h light/8 h dark, 22 °C). After 10 d, hypocotyl length was recorded. For adult plants, four-week-old WT and *MaDTX19*-OE *Arabidopsis* were sprayed with 0.5 μmol·L^{-1} IAA solution containing 0.01% Tween-20, and control plants received the same solution without IAA. Fresh weight and dry weight were measured 7 d after treatment, with at least 15 seedlings or ten adult plants per genotype and treatment.

Statistical analysis

All experiments were performed with at least three independent biological replicates. Data are presented as the mean ± standard deviation (SD). Statistical analyses were performed using SPSS software (v20.0). Student's *t*-test was applied for comparisons between two groups. One-way analysis of variance (ANOVA) followed by Duncan's multiple range test was used for multiple-group comparisons. Different lowercase letters or asterisks indicate statistically significant differences (* $p < 0.05$; ** $p < 0.01$; *** $p < 0.001$).

Results

Identification and molecular characterization of the Al^{3+}-inducible MATE transporter *MaDTX19*

To identify key MATE family members involved in Al^{3+} stress responses, we analyzed transcriptomic data from Al^{3+}-stressed mulberry seedlings. Among the six MATE family members whose transcript abundance was upregulated under Al^{3+} stress, *MaDTX19*

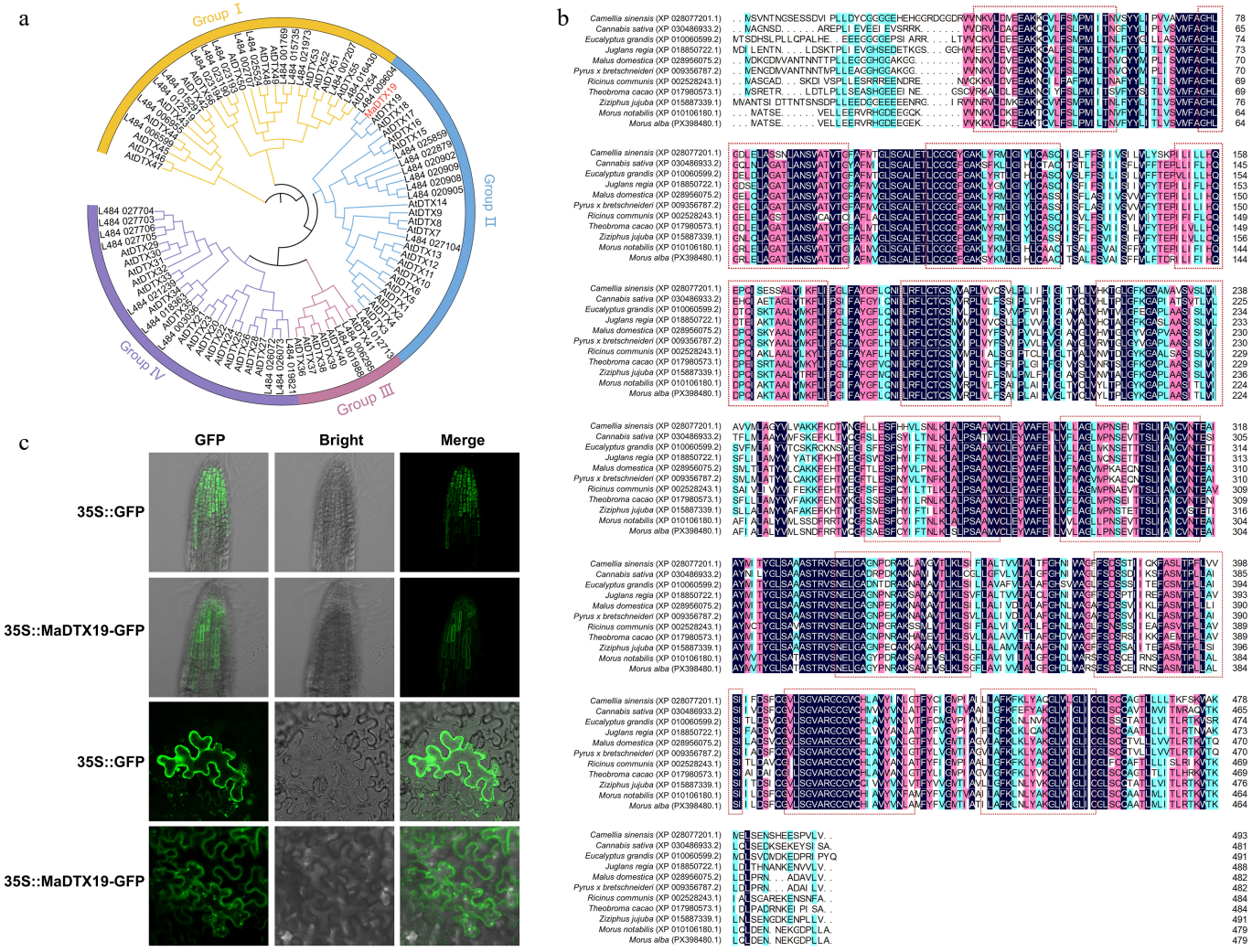


Fig. 1 Molecular characterization and subcellular localization of MaDTX19. (a) Phylogenetic analysis of MaDTX19 and MATE family proteins from *Arabidopsis* and mulberry. The phylogenetic tree was constructed using the neighbor-joining method with 1,000 bootstrap replicates. MaDTX19 (highlighted in red) clusters within MATE Group II with AtDTX18 and AtDTX19. (b) Transmembrane domain prediction of MaDTX19 and its homologs. The transmembrane regions are marked with dashed boxes. (c) Subcellular localization of MaDTX19 in *N. benthamiana* leaf epidermal cells and *Arabidopsis* root tips.

exhibited the most pronounced upregulation (Supplementary Fig. S1). Phylogenetic analysis placed MaDTX19 within Group II of the MATE family, closely related to *Arabidopsis* AtDTX18 and AtDTX19 (Fig. 1a). MaDTX19 contains 12 typical transmembrane domains (Fig. 1b) and localizes to the plasma membrane (Fig. 1c), consistent with a role in substrate efflux.

RT-qPCR analysis demonstrated that *MaDTX19* transcript levels were rapidly and strongly induced by Al^{3+} stress (Fig. 2a). Treatments with ABA and IAA also significantly upregulated *MaDTX19* expression (Fig. 2b, c), suggesting integration with both stress and hormonal signaling pathways. Promoter-GUS analysis in transgenic *Arabidopsis* further showed that *pMaDTX19* activity was markedly enhanced by Al^{3+}, ABA, and IAA treatments (Fig. 2d). These results establish *MaDTX19* as an Al^{3+}-inducible MATE gene responsive to multiple stress-related signals.

Ectopic expression of *MaDTX19* suppresses growth and development

To explore whether *MaDTX19* affects plant development, we heterologously expressed it in *Arabidopsis*. Under both continuous light and dark conditions, transgenic seedlings exhibited significantly shorter hypocotyls compared to wild-type (WT) (Fig. 3a, b). When grown under standard photoperiods, mature *MaDTX19*-overexpressing (OE) plants displayed a striking dwarf phenotype with reduced plant height and total biomass (fresh and dry weight) (Fig. 3c–f). Moreover, reproductive development was also impaired in transgenic lines, as evidenced by shorter siliques and lower thousand-seed weight (Fig. 3g–i). Thus, MaDTX19 acts as a negative regulator of plant growth and development.

MaDTX19 confers Al^{3+} tolerance by enhancing citrate secretion and antioxidant capacity

To assess the role of *MaDTX19* in Al^{3+} stress tolerance, germination and growth phenotypes of WT and *MaDTX19*-OE *Arabidopsis* seedlings under $AlCl_3$ stress were compared. Transgenic seeds exhibited significantly higher germination rates and faster germination kinetics than WT (Fig. 4a), and OE seedlings maintained longer primary roots across multiple Al^{3+} concentrations (Fig. 4b, c), confirming that *MaDTX19* confers Al^{3+} tolerance at the seedling stage. Under Al^{3+} stress, OE lines accumulated higher citrate levels in root tips (Fig. 4d) and showed less Al^{3+} accumulation in the meristematic zone by hematoxylin staining (Fig. 4e). We further examined Al^{3+} distribution at the whole-plant level. Both root and shoot Al^{3+} contents were significantly lower in OE lines compared to WT, with a more pronounced reduction in shoots. Consequently, the translocation factor (shoot Al^{3+}/root Al^{3+} ratio) was markedly reduced in transgenic plants (Fig. 4f), suggesting that MaDTX19 reduces both Al^{3+} uptake by roots and subsequent translocation to shoots by enhancing chelation or compartmentalization within root tissues.

Under Al^{3+} stress, OE plants exhibited milder chlorosis and wilting, with significantly higher survival rates than WT (Fig. 5a, b). Physiological analyses showed that OE plants accumulated higher levels of proline (Fig. 5c) and maintained lower MDA levels (Fig. 5d). Chlorophyll fluorescence measurements showed that the maximum photochemical efficiency of photosystem II (Fv/Fm) was significantly higher in transgenic plants (Fig. 5e, f), indicating that *MaDTX19* overexpression effectively alleviated the Al^{3+}-induced inhibition of photosystem II photochemical efficiency. ROS staining showed weaker DAB and NBT signals in OE leaves under Al^{3+} stress

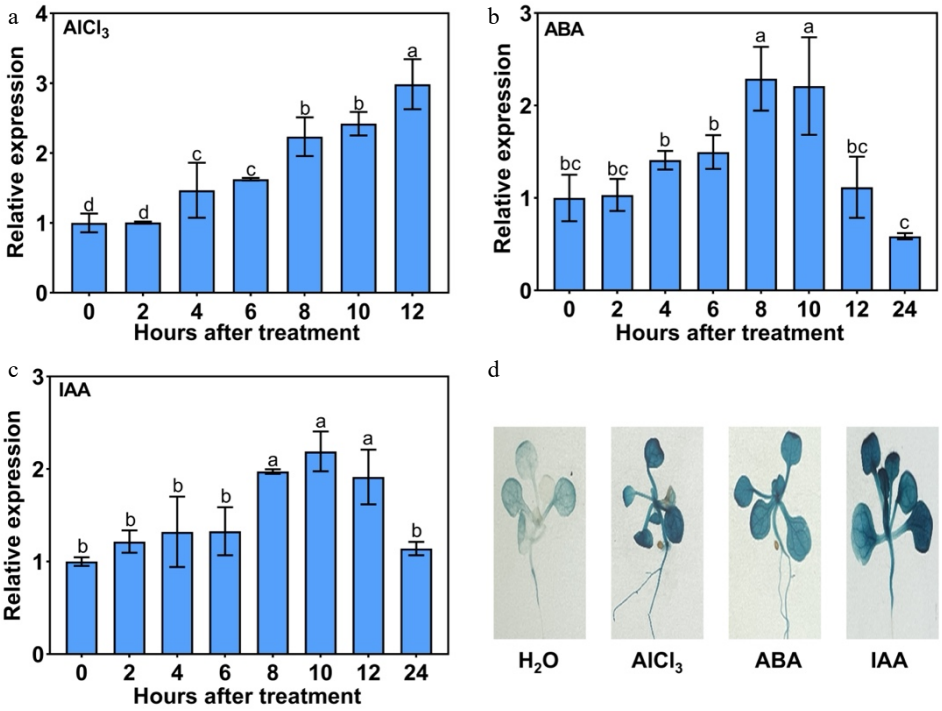


Fig. 2 Expression pattern of *MaDTX19* in response to Al^{3+} stress and phytohormone treatments. (a) Time-course analysis of *MaDTX19* transcript levels in mulberry seedlings under 80 mmol·L^{-1} Al^{3+} stress, detected by RT-qPCR. *MaDTX19* expression in mulberry seedlings treated with (b) 50 μmol·L^{-1} ABA and (c) 50 μmol·L^{-1} IAA. (d) GUS staining analysis of *pMaDTX19::GUS* transgenic *Arabidopsis* seedlings under different treatments (H_2O, 0.8 mmol·L^{-1} $AlCl_3$, 50 μmol·L^{-1} ABA, 50 μmol·L^{-1} IAA). All RT-qPCR data are presented as mean ± SD of three biological replicates with three technical replicates each. Different letters indicate significant differences ($p < 0.05$).

https://doi.org/10.48130/forres-0026-0031

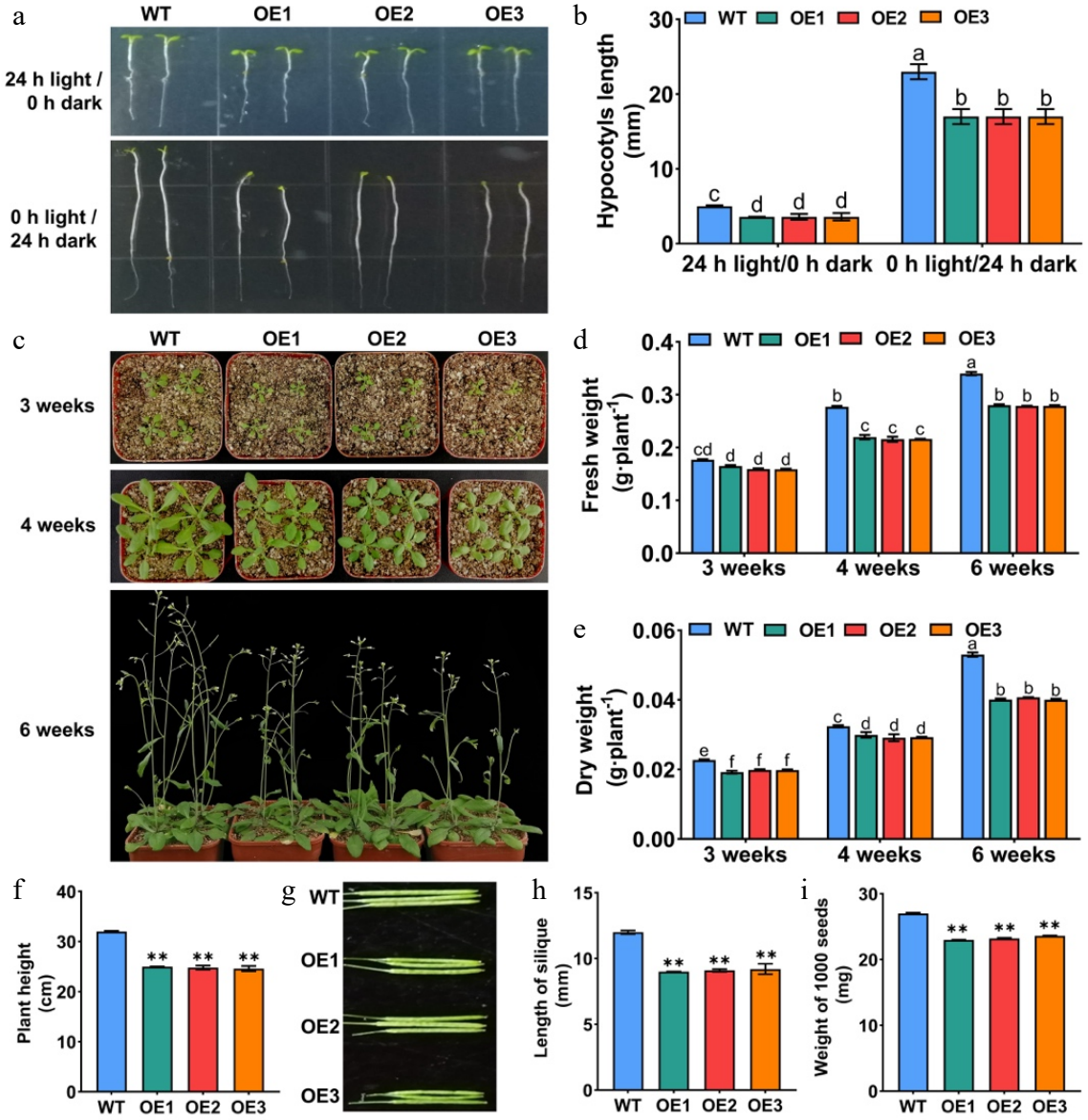


Fig. 3 Ectopic expression of *MaDTX19* suppresses plant growth and development in *Arabidopsis*. (a) Hypocotyl phenotypes of seven-day-old wild-type (WT) and *MaDTX19*-overexpressing (OE) *Arabidopsis* seedlings grown under (a) continuous light (24 h light/0 h dark) and dark (0 h light/24 h dark) conditions. (b) Hypocotyl length of seven-day-old WT and OE *Arabidopsis* seedlings grown under continuous light and dark. (c) Representative phenotypes of WT and *MaDTX19*-OE plants under standard photoperiod. Quantitative analysis of growth and reproductive traits: (d) fresh weight, (e) dry weight, (f) plant height, (g) silique phenotype, (h) silique length, and (i) thousand-seed weight. Data represent the mean ± SD. Asterisks indicate significant differences between WT and OE transgenic lines (*t*-test, ** $p < 0.01$). Different letters indicate statistically significant differences among treatments ($p < 0.05$).

(Fig. 5g), accompanied by higher activities of CAT, SOD, and POD (Fig. 5h–j). These findings indicate that *MaDTX19* confers Al^{3+} tolerance by enhancing antioxidant capacity and maintaining redox homeostasis.

To determine whether the degree of growth inhibition correlates with Al^{3+} tolerance, we examined multiple independent transgenic lines with graded *MaDTX19* expression levels. Lines with greater growth suppression exhibited higher survival rates and proline content, but lower MDA accumulation under Al^{3+} stress (Fig. 5k–o). This relationship plateaued beyond a certain expression threshold, suggesting an optimal MaDTX19 activity level that maximizes tolerance while minimizing fitness costs. These data indicate that growth inhibition and Al^{3+} tolerance are dosage-dependently coupled.

MaDTX19 promotes the accumulation of anthocyanin and proanthocyanidin

Given that some MATE transporters mediate vacuolar sequestration of flavonoids, we examined whether MaDTX19 influences this pathway. *MaDTX19*-OE seedlings grown on sucrose-containing medium exhibited notably darker cotyledon pigmentation (Fig. 6a) and significantly increased anthocyanin accumulation (Fig. 6b). Leaves and petioles of OE seedlings exhibited deeper purple-red coloration, with significantly increased anthocyanin levels (Fig. 6c). DMACA staining of seed coats revealed intensified magenta staining in OE seeds (Fig. 6d), indicating enhanced proanthocyanidin biosynthesis. These results demonstrate that *MaDTX19* enhances anthocyanin accumulation.

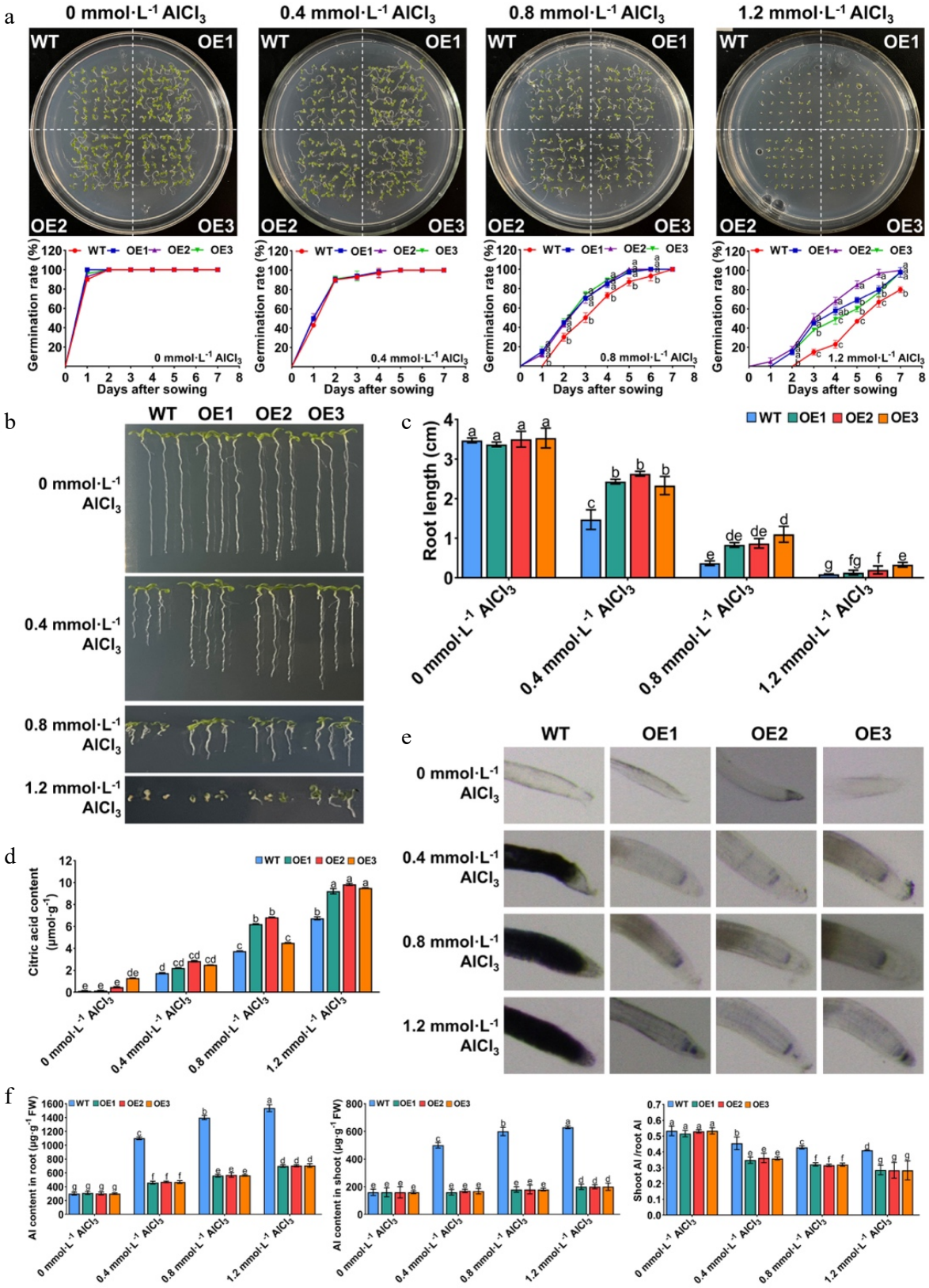


Fig. 4 MaDTX19 enhances Al^{3+} tolerance by promoting citrate secretion and reducing Al^{3+} accumulation in transgenic *Arabidopsis*. (a) Germination kinetics of WT and *MaDTX19*-OE seeds under 0, 0.4, 0.8, 1.2 mmol·L^{-1} $AlCl_3$ stress. Germination rate was recorded daily for 7 d. Primary root length of seedlings grown on MS medium supplemented with (b) 0, 0.4, 0.8, 1.2 mmol·L^{-1} $AlCl_3$ and (c) its quantitative analysis. (d) Citrate content in root tips under $AlCl_3$ stress. (e) Hematoxylin staining of root tips (red color indicates Al^{3+} accumulation). (f) Al^{3+} content in roots and shoots, and the calculated translocation factor (shoot Al^{3+}/root Al^{3+} ratio) of WT and OE lines under Al^{3+} stress. OE1-3 represent different *MaDTX19*-OE lines. Data are presented as mean ± SD. Different lowercase letters above bars indicate significant differences ($p < 0.05$).

https://doi.org/10.48130/forres-0026-0031

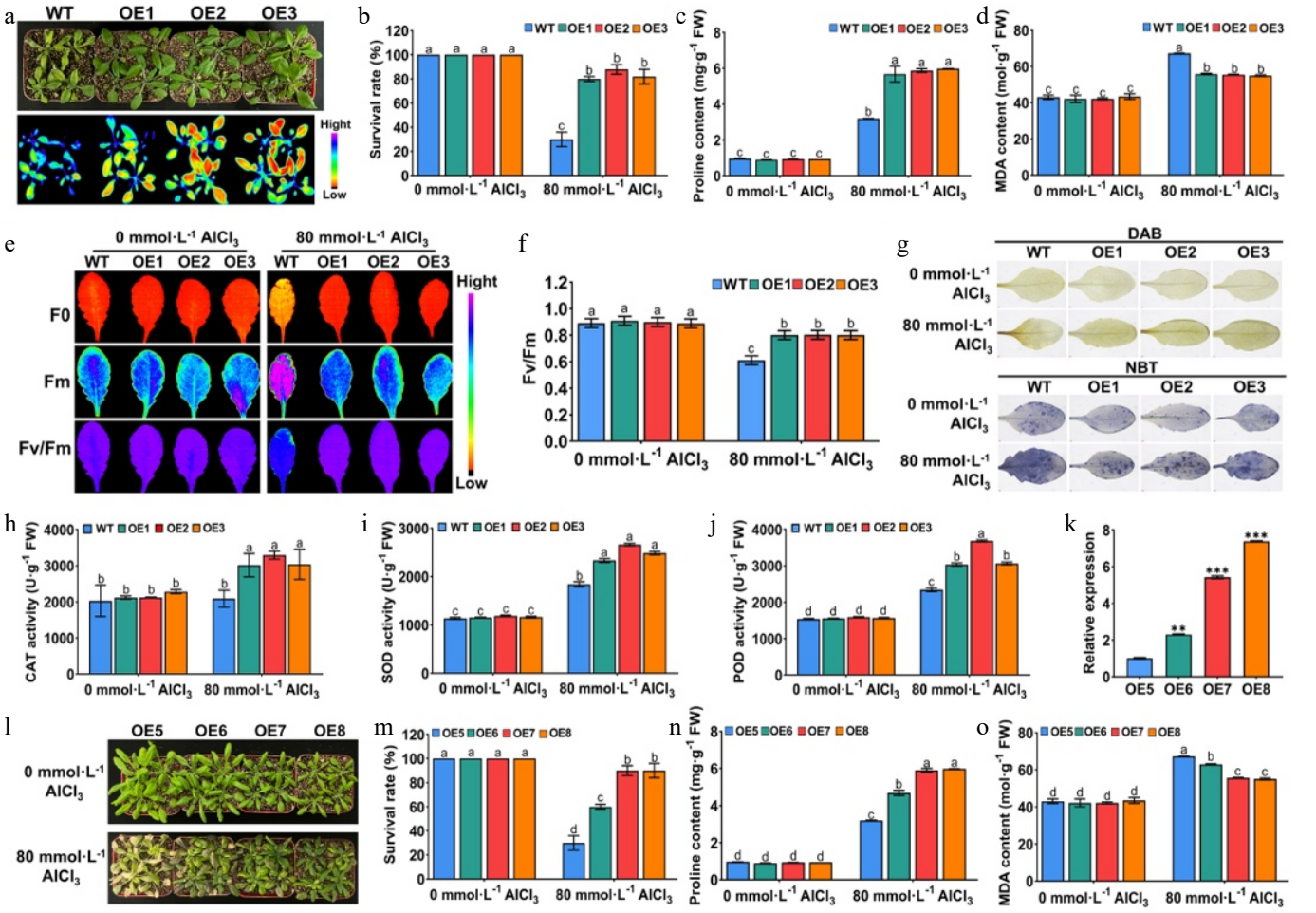


Fig. 5 MaDTX19 confers Al^{3+} tolerance by enhancing antioxidant capacity and protecting photosynthetic function in transgenic *Arabidopsis*. (a) Phenotypes and chlorophyll fluorescence images and (b) survival rate of four-week-old WT and *MaDTX19*-OE plants under 80 mmol·L^{-1} $AlCl_3$ stress. (c) Proline and (d) MDA content in leaves under $AlCl_3$ stress. (e) Chlorophyll fluorescence images and (f) quantitative analysis of maximum photochemical efficiency of PSII (Fv/Fm). (g) Histochemical staining of H_2O_2 (DAB) and O_2^{-} (NBT) in leaves under $AlCl_3$ stress. (h) Activities of CAT, (i) SOD, and (j) POD in leaves under $AlCl_3$ stress. Correlation analysis of growth inhibition and Al^{3+} tolerance in transgenic lines with graded *MaDTX19* expression levels: relative expression of MaDTX19 in (k) independent OE lines, (l) phenotypes under Al^{3+} stress, (m) survival rate, (n) proline content, and (o) MDA accumulation. OE1-8 represent different *MaDTX19*-OE lines. Data are presented as mean ± SD. Different lowercase letters above bars indicate significant differences ($p < 0.05$).

MaDTX19 enhances Al^{3+} tolerance in mulberry hairy roots

To validate the function of *MaDTX19* in its native woody species, we generated *A. rhizogenes*-mediated hairy root transformations in mulberry. Under Al^{3+} stress, seedlings harboring *MaDTX19*-OE hairy roots showed milder symptoms than empty-vector controls, which displayed severe chlorosis and wilting (Fig. 7a). ROS accumulation was substantially lower in transgenic leaves (Fig. 7b), corresponding with higher activities of POD, SOD, and CAT (Fig. 7c–e) and higher Fv/Fm values (Fig. 7f, g). Survival rate assays confirmed that *MaDTX19*-OE hairy root lines had a higher survival rate than controls under prolonged Al^{3+} exposure (Fig. 7h). Hematoxylin staining demonstrated significantly less Al^{3+} accumulation in the root meristematic zones of transgenic hairy roots (Fig. 7i), accompanied by elevated citrate content in root tips (Fig. 7j). Taken together, these findings demonstrate that *MaDTX19* confers Al^{3+} tolerance in mulberry through both ROS scavenging and citrate-mediated Al^{3+} chelation.

Al^{3+} stress induces MaDTX19 phosphorylation at Ser4

Bioinformatic analysis predicted that the fourth serine residue (Ser4) of MaDTX19 is a potential phosphorylation site. Using a phospho-specific antibody, we detected increased phosphorylation of MaDTX19 in OE *Arabidopsis* roots with prolonged Al^{3+} treatment (Fig. 8a), confirming stress-induced phosphorylation at Ser4. To further investigate the regulatory effect of Ser4 phosphorylation on MaDTX19 protein stability, we generated phosphodeficient (Ser4-to-Ala, SA) and phosphomimetic (Ser4-to-Asp, SD) mutants. Western blot analysis using a GFP antibody indicated that the abundance of MaDTX19-GFP and $MaDTX19^{SD}$-GFP increased gradually under Al^{3+} stress, whereas $MaDTX19^{SA}$-GFP showed no obvious changes (Fig. 8b). Thus, the Ser4 site of MaDTX19 serves as a phosphorylation modification site in response to Al^{3+} stress, with its phosphorylation status directly regulating MaDTX19 protein stability.

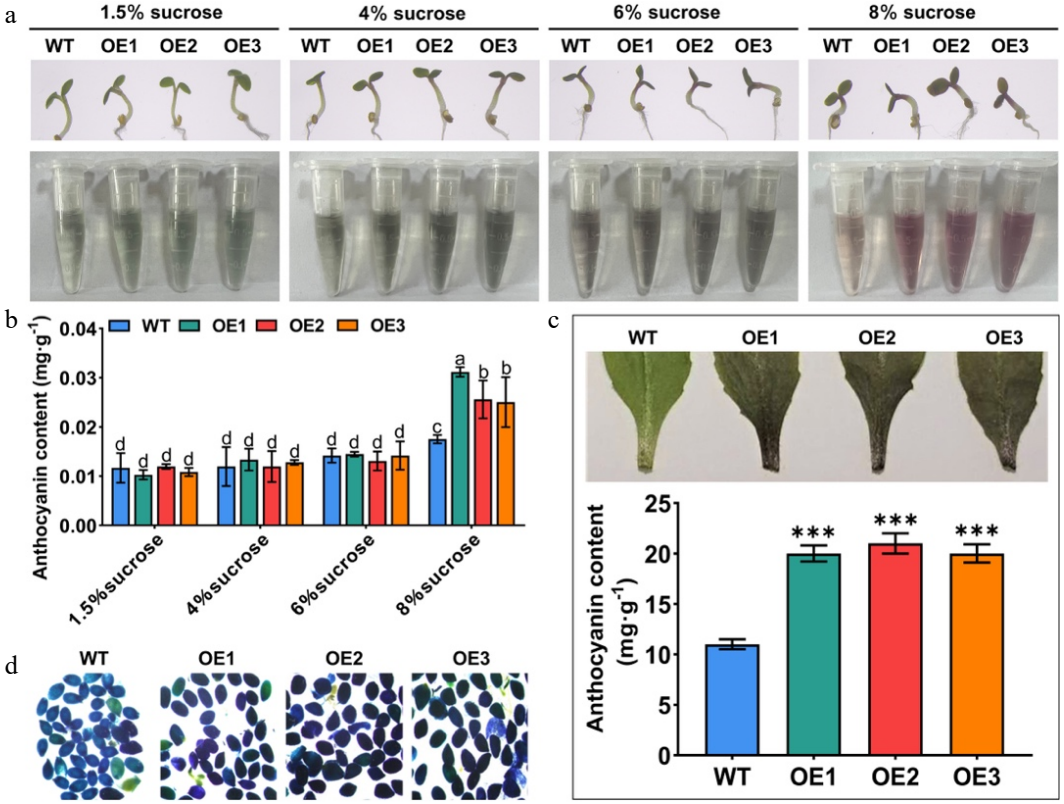


Fig. 6 MaDTX19 promotes anthocyanin and proanthocyanidin accumulation in transgenic *Arabidopsis*. (a) Cotyledon phenotypes and (b) quantitative analysis of anthocyanin content of WT and *MaDTX19*-OE seedlings grown on MS medium with 1.5%, 4%, 6%, and 8% sucrose. (c) Phenotypes and anthocyanin content of leaves and petioles of WT and *MaDTX19*-OE *Arabidopsis* seedlings. (d) DMACA staining of proanthocyanidins in seed coats (magenta color indicates proanthocyanidin accumulation). OE1-3 represent different *MaDTX19*-OE lines. Data represent the mean ± SD. Asterisks denote significant differences (*t*-test, *** $p < 0.001$), while different letters indicate significant differences at $p < 0.05$.

Ser4 phosphorylation is required for both growth suppression and Al^{3+} tolerance

To explore whether Ser4 phosphorylation is functionally required, we transformed MaDTX19, MaDTX19^{SA}, and MaDTX19^{SD} constructs into *Arabidopsis*. Phenotypic analyses showed that both *MaDTX19* and *MaDTX19^{SD}* overexpressing plants exhibited growth inhibition compared to WT plants, characterized by reduced rosette leaf number and shorter siliques. In contrast, *MaDTX19^{SA}* overexpressing plants showed no significant difference from WT (Fig. 9a, b). These results demonstrate that Ser4 phosphorylation is indispensable for the growth regulatory function of MaDTX19.

In Al^{3+} tolerance assays, both *MaDTX19* and *MaDTX19^{SD}* overexpressing plants exhibited significantly enhanced Al^{3+} tolerance, with higher seed germination rates and longer primary roots compared to WT. In contrast, the *MaDTX19^{SA}* overexpressing plants showed Al^{3+} sensitivity comparable to WT, with lower germination rates and shorter roots (Fig. 9c). In addition, the primary roots of *MaDTX19* and *MaDTX19^{SD}* overexpressing seedlings were shorter than WT plants under Al^{3+} stress (Fig. 9d, e). These results demonstrate that Ser4 phosphorylation is indispensable for both growth suppression and Al^{3+} tolerance.

Phosphorylation enhances MaDTX19 interaction with auxin-related proteins

To elucidate the mechanistic basis of the phosphorylation-dependent switch, we examined the MaDTX19 interaction network. Membrane yeast two-hybrid, BiFC, and LCA assays revealed that MaDTX19 interacts with three auxin-related proteins: the auxin-induced protein Ma5NG4, the auxin-responsive protein MaWAT1, and the auxin efflux carrier component MaAECC8 (Fig. 10a–c). Importantly, the phosphomimetic MaDTX19^{SD} mutant exhibited markedly stronger interaction with Ma5NG4, MaWAT1, and MaAECC8. Conversely, the phosphodeficient MaDTX19^{SA} mutant showed significantly weakened binding (Fig. 10d). Thus, Ser4 phosphorylation enhances MaDTX19 association with auxin transport components, likely disrupting auxin homeostasis and accounting for growth inhibition.

MaDTX19 alters auxin homeostasis and spatial distribution in root tips

Using the auxin-responsive reporter DR5::GFP, we analyzed auxin distribution in root tips. Under Al^{3+}-free conditions, weak GFP fluorescence signals were confined to the meristematic and elongation zones of WT root tips, where auxin levels remained basal. In *MaDTX19*-OE plants, GFP fluorescence was markedly stronger and extended beyond these growth zones into non-growing tissues, including the root epidermis and cortex. Under Al^{3+} stress, GFP fluorescence intensity increased and spread to non-growing regions in both WT and *MaDTX19*-OE root tips, with stronger enhancement and wider spreading in *MaDTX19*-OE roots than in WT (Fig. 11a). Quantification showed higher auxin content in *MaDTX19*-OE root tips under both conditions (Fig. 11b). These results indicate that *MaDTX19* overexpression causes auxin redistribution, with increased accumulation in non-growing regions and altered auxin distribution in the meristematic zone. This likely depletes the auxin pool required for cell division and elongation, providing a mechanistic explanation for the observed dwarf phenotype.

https://doi.org/10.48130/forres-0026-0031

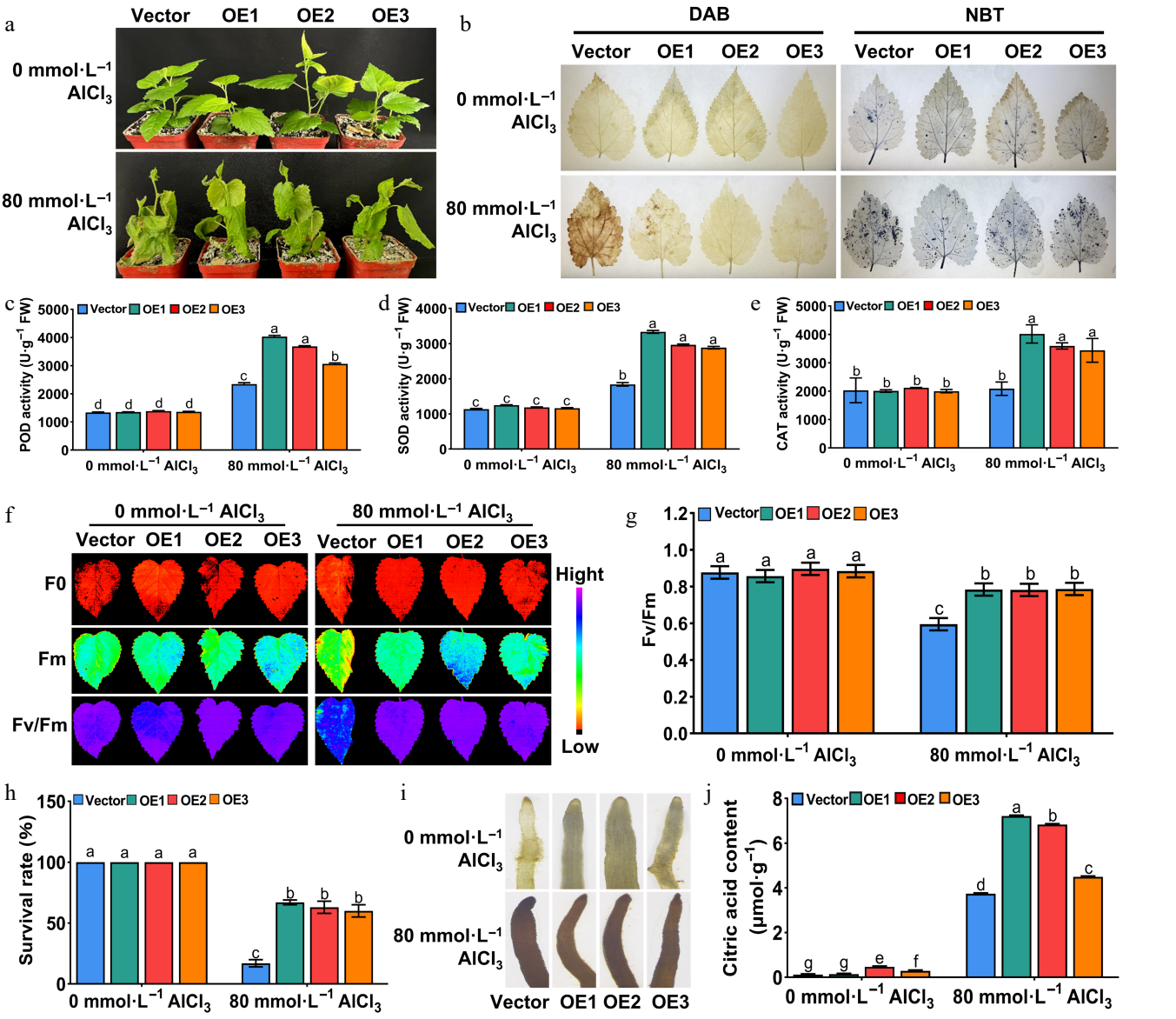


Fig. 7 Overexpression of *MaDTX19* enhances Al^{3+} tolerance in hairy root-transformed mulberry seedlings. (a) Phenotypes of empty vector (Vector) control and *MaDTX19*-OE (OE1-3) mulberry seedlings under 80 mmol·L^{-1} $AlCl_3$ stress. (b) DAB and NBT staining of mulberry leaves under $AlCl_3$ stress. (c) POD, (d) SOD, and (e) CAT activities in leaves under $AlCl_3$ stress. (f) Chlorophyll fluorescence images and (g) Fv/Fm values of seedlings under $AlCl_3$ stress. (h) Survival rate of seedlings under $AlCl_3$ stress. (i) Hematoxylin staining of hairy root tips. (j) Citrate content in hairy root tips under $AlCl_3$ stress. Data represent mean ± SD. Different letters indicate significant differences ($p < 0.05$).

To test whether auxin supplementation could rescue the growth defect, we applied exogenous IAA to WT and *MaDTX19*-OE seedlings under standard light conditions. IAA treatment slightly promoted growth in both genotypes, as reflected by modest increases in hypocotyl length, fresh weight, and dry weight. However, OE seedlings remained significantly smaller than WT controls across all measured parameters, with no obvious rescue of the dwarf morphology (Fig. 11c–g). This limited recovery is consistent with auxin mislocalization rather than simple auxin deficiency as the primary defect, as exogenous IAA would still be subject to the same disrupted polar transport machinery.

A MaMYB61/MaMYB308 transcriptional module fine-tunes *MaDTX19* expression

Bioinformatic analysis predicted that MaMYB61 potentially binds to the *MaDTX19* promoter (*pMaDTX19*). Y1H assays confirmed direct binding of MaMYB61 to *pMaDTX19* (Fig. 12a), and LUC reporter assays demonstrated that MaMYB61 significantly enhanced *pMaDTX19* activity (Fig. 12b, c), suggesting a positive regulatory role of MaMYB61 in *MaDTX19* expression. EMSA further confirmed sequence-specific binding of MaMYB61 to the promoter (Fig. 12d).

Previous studies reported interactions between MYB61 and MYB308 in plants. Physical interaction between MaMYB61 and MaMYB308 was detected by Y2H assays (Fig. 12e) and further confirmed by LCA (Fig. 12f). BiFC analysis additionally showed that the two proteins interacted within the nucleus (Fig. 12g). Intriguingly, LUC assays showed that MaMYB308 attenuated MaMYB61-mediated transactivation of *pMaDTX19* (Fig. 12h). These results define a MaMYB61-MaMYB308 transcriptional module in which MaMYB61 activates and MaMYB308 represses *MaDTX19* expression, enabling dynamic fine-tuning in response to stress intensity.

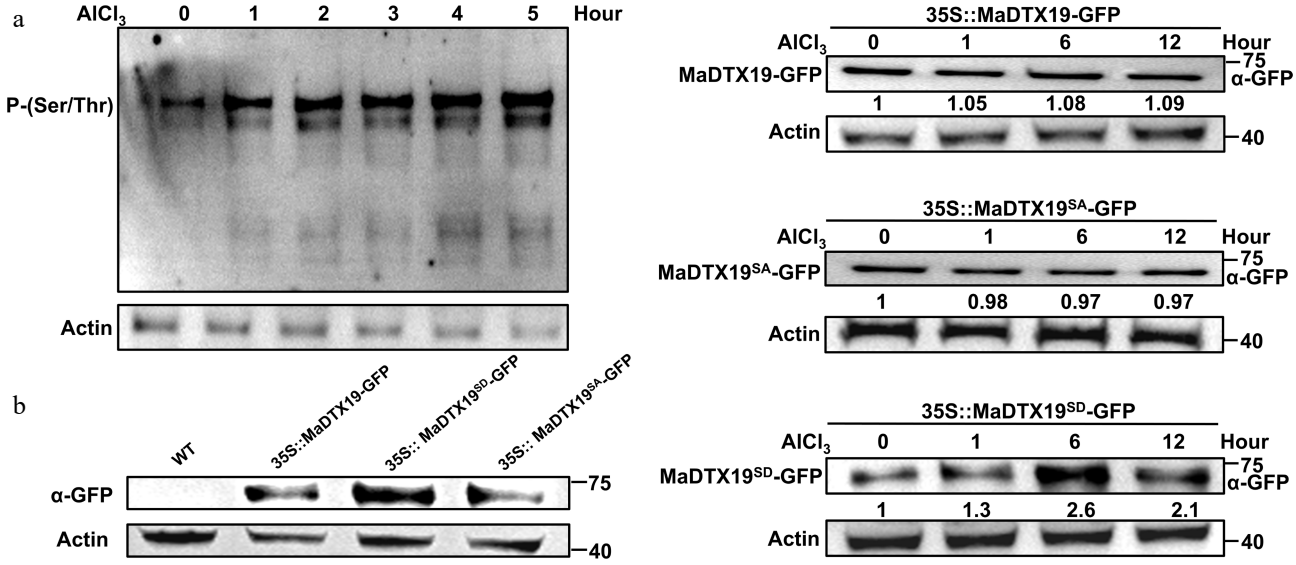


Fig. 8 Al^{3+} stress induces *in vivo* phosphorylation of MaDTX19 at Ser4 and modulates its protein stability. (a) Time-course analysis of Ser4 phosphorylation level of MaDTX19 in *MaDTX19*-OE *Arabidopsis* root tips under 0.8 mmol·L^{-1} $AlCl_3$ stress, detected by western blot using an anti-phospho-(Ser/Thr) antibody. (b) Protein stability of MaDTX19-GFP, MaDTX19^{SA}-GFP, and MaDTX19^{SD}-GFP in *Arabidopsis* root tips under $AlCl_3$ stress detected by western blot using an anti-GFP antibody.

Discussion

Balancing growth and defense is a fundamental challenge for plants, especially long-lived perennials like mulberry that face persistent abiotic stresses, yet the molecular mechanisms governing this balance remain incompletely understood. While transcription factors and hormone signals are well-documented regulators of the growth-defense balance, relatively few studies have explored how transporters integrate stress signals and allocate resources through post-translational modifications[1,2]. Here, we show that MaDTX19 functions as a phosphorylation-dependent molecular hub that mediates resource reallocation from growth to defense under Al^{3+} stress. Two interconnected regulatory layers, Ser4 phosphorylation and transcriptional control by the MaMYB61-MaMYB308 module, coordinate this trade-off in a woody perennial.

Ser4 phosphorylation integrates growth suppression with Al^{3+} tolerance

The ability of a single phosphorylation event at Ser4 to govern both growth inhibition and Al^{3+} tolerance distinguishes MaDTX19 from previously characterized MATE transporters. Transcriptional upregulation of MATE genes such as *SbMATE* and *HvAACT1* enhances citrate secretion and Al^{3+} exclusion, but these transporters do not simultaneously modulate plant growth[16,34,35,42]. MaDTX19 achieves dual functionality through phosphorylation-dependent rewiring of its protein interaction network. The phosphorylated form binds more strongly to auxin-related proteins (Ma5NG4, MaWAT1, MaAECC8), disrupting auxin transport and suppressing growth while concurrently activating Al^{3+} tolerance pathways. This phosphorylation-dependent switch enables coordinated suppression of growth and activation of detoxification.

The biological significance of this switch lies in its temporal advantage. Transcriptional reprogramming takes time, whereas reversible phosphorylation acts within minutes[12,29,30,43]. For plants experiencing acute Al^{3+} toxicity, where root elongation is inhibited within 30 min of stress onset, a phosphorylation-dependent switch provides an immediate mechanism for resource reallocation[23,27]. This rapid response is particularly relevant for woody perennials that cannot escape stress. The reversibility of phosphorylation also allows growth to resume quickly once stress subsides.

Recent studies have documented phosphorylation-dependent regulation of MATE transporters in other species, but these focus on modulation of transport activity rather than coordination of growth-defense trade-offs[12,18,23]. MaDTX19 therefore represents a distinct paradigm, wherein phosphorylation toggles between growth and defense modes through rewiring of protein-protein interactions. We acknowledge that the upstream kinase responsible for Ser4 phosphorylation remains unidentified. Given that ABA induces *MaDTX19* expression, ABA signaling may participate in activating this kinase, although direct evidence is lacking. We also recognize that our auxin distribution data establish a strong correlation with growth inhibition, but we cannot exclude the possibility that some auxin changes are secondary consequences of broader physiological alterations.

Dual detoxification pathways and transcriptional fine-tuning

MaDTX19 confers Al^{3+} tolerance through two synergistic pathways, citrate secretion and flavonoid-mediated antioxidant defense. Citrate secreted into the rhizosphere chelates Al^{3+} and reduces its entry into root cells, while the flavonoid-antioxidant system scavenges residual ROS[6,16,17,21,23,31]. This outside-in strategy mirrors the detoxification logic observed in other Al^{3+}-tolerant species. Integration of both pathways through a single phosphorylation-dependent transporter distinguishes MaDTX19 from other MATE family members. In contrast to MaDTX19, which consolidates citrate secretion, flavonoid accumulation, and growth modulation into one phosphorylation-gated protein, SbMATE functions primarily as a citrate transporter[44], AtDTX50 participates in ABA efflux[32], and BoMATE enhances Al^{3+} tolerance but imposes a growth penalty[31].

https://doi.org/10.48130/forres-0026-0031

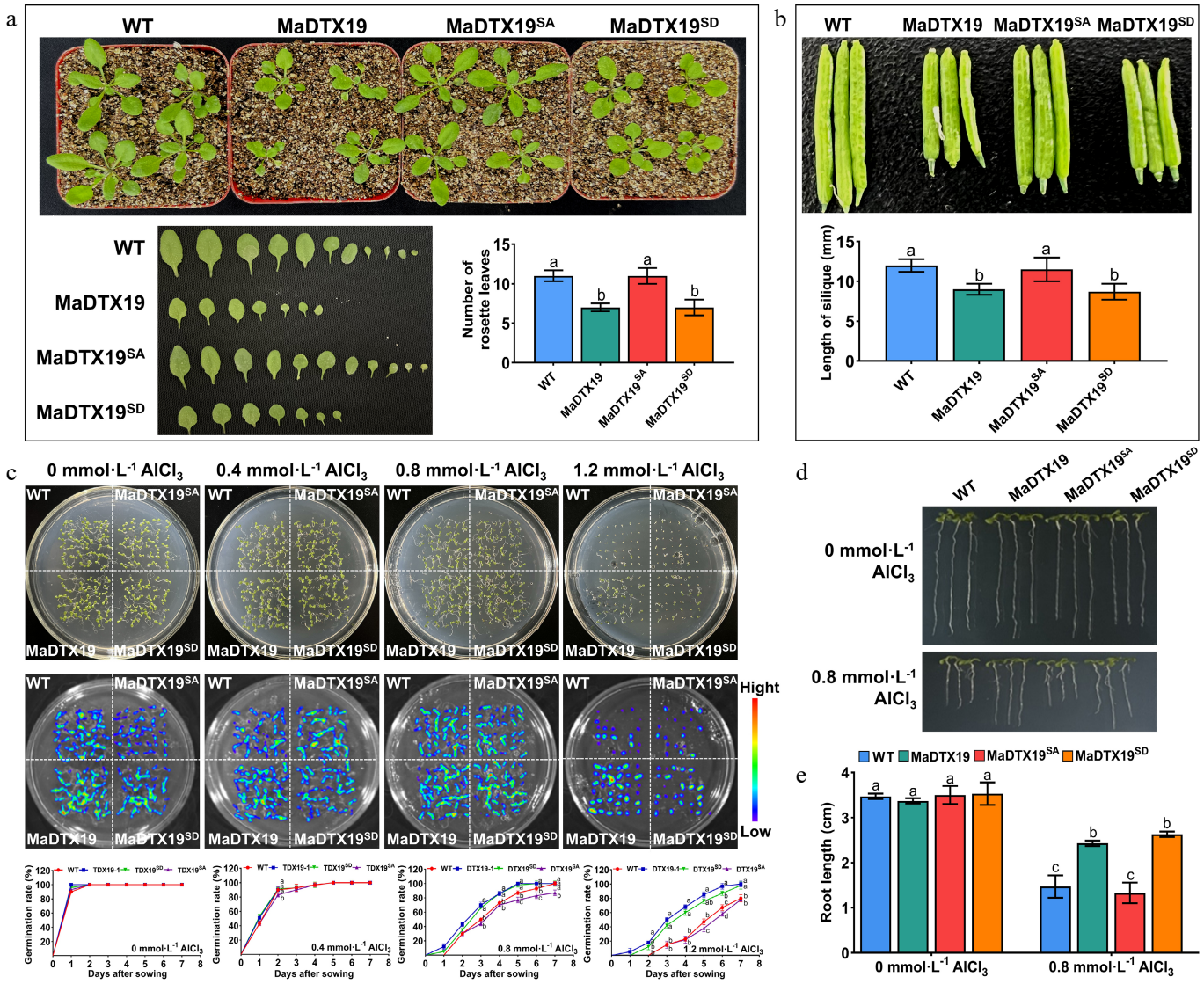


Fig. 9 Ser4 phosphorylation is essential for MaDTX19-mediated growth inhibition and Al^{3+} tolerance. (a) Growth phenotypes of four-week-old WT, *MaDTX19*-OE, *MaDTX19*^{SD}-OE, and *MaDTX19*^{SA}-OE *Arabidopsis* under normal conditions. (b) Silique length of the same plants under normal conditions. (c) Seed germination rate under 0, 0.4, 0.8, 1.2 mmol·L^{-1} $AlCl_3$ stress. (d) Primary root phenotypes of seedlings grown on MS medium supplemented with 0 or 0.8 mmol·L^{-1} $AlCl_3$. (e) Primary root length of seedlings on MS medium supplemented with 0 or 0.8 mmol·L^{-1} $AlCl_3$. Different lowercase letters above the bars indicate statistically significant differences among treatments ($p < 0.05$).

The MaMYB61-MaMYB308 transcriptional module adds an additional layer of regulation. MaMYB61 activates *MaDTX19* transcription, while MaMYB308 attenuates this activation through protein-protein interaction. This activator-repressor configuration is conceptually analogous to the MYC2-MYB21/24 module in JA signaling. The temporal dynamics of this module are particularly informative. *MaMYB61* is rapidly induced by Al^{3+}, whereas *MaMYB308* shows delayed induction, consistent with a negative feedback mechanism that curtails excessive *MaDTX19* expression once the acute response is mounted (Supplementary Fig. S2). Compared to STOP1, which directly activates multiple MATE genes in *Arabidopsis* and other species, the MYB61-MYB308 module represents a distinct regulatory architecture employing an activator-repressor pair for dynamic expression tuning. Our Y1H, LUC, and EMSA assays confirm that MaMYB61 directly binds and activates the MaDTX19 promoter. We acknowledge that increased citrate and flavonoid levels, while consistent with a role for MaDTX19 in their transport, do not constitute direct biochemical evidence of transport activity. Direct transport assays are needed to establish substrate specificity.

A two-tier strategy for environmental plasticity and the adaptive trade-off

Based on these findings, we propose a working model for MaDTX19-mediated regulation of the growth-defense continuum in mulberry (Fig. 13). Under optimal conditions, low *MaDTX19* expression and basal Ser4 phosphorylation maintain normal auxin transport and growth. Upon Al^{3+} stress, the MaMYB61-MaMYB308 module rapidly induces *MaDTX19* transcription, while a yet-unidentified kinase phosphorylates Ser4, switching MaDTX19 to its active conformation. Phosphorylated MaDTX19 then exerts dual functions, inhibiting growth by interacting with auxin transport components

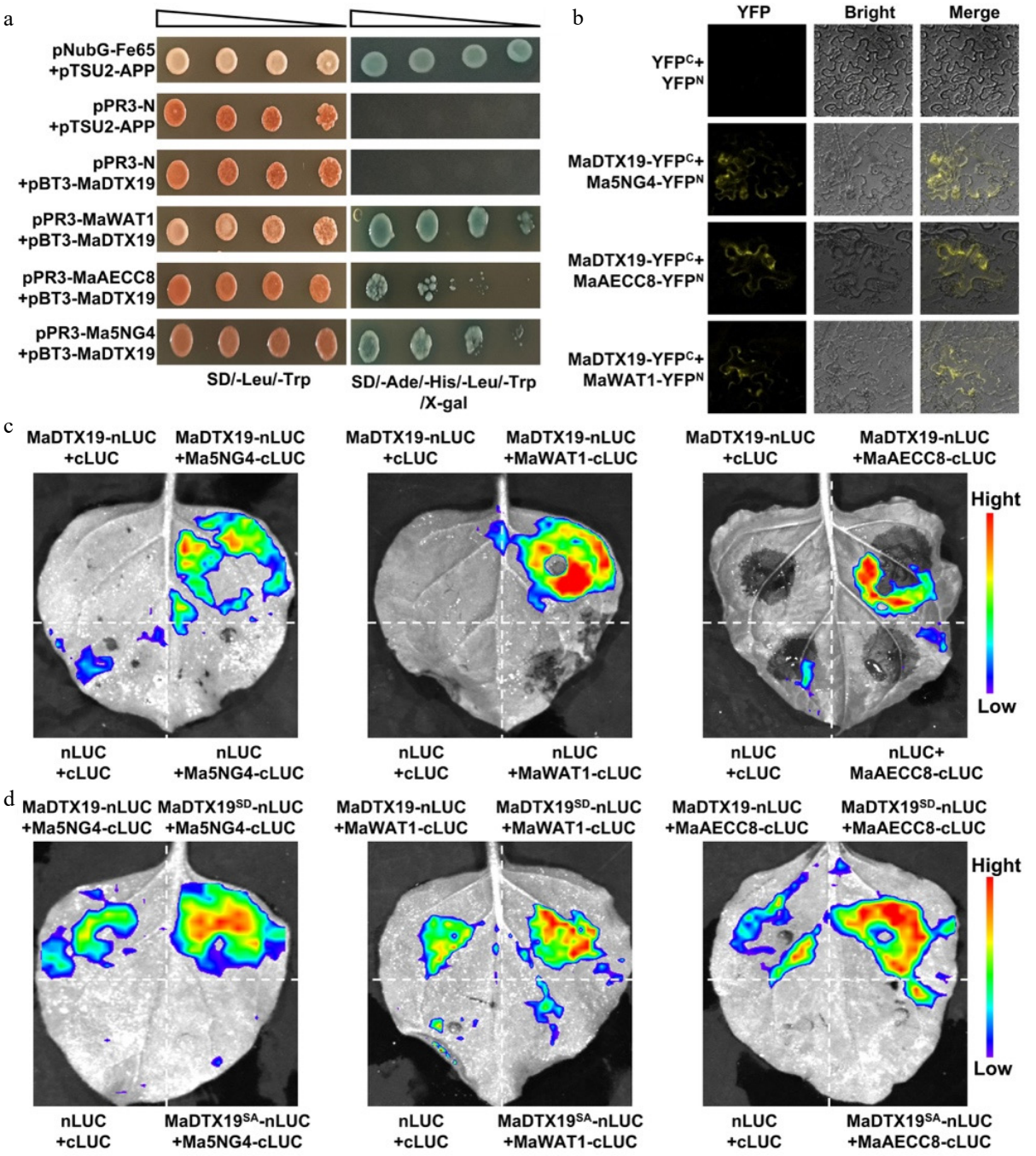


Fig. 10 Ser4 phosphorylation enhances the interaction of MaDTX19 with auxin-related proteins. (a) Membrane yeast two-hybrid assay showing the interaction of MaDTX19 with Ma5NG4, MaWAT1, and MaAECC8. Growth on QDO medium indicates a positive interaction. (b) Bimolecular fluorescence complementation (BiFC) assay confirming the interactions in *N. benthamiana* leaf epidermal cells. YFP fluorescence indicates protein-protein interaction. (c) Luciferase complementation assay (LCA) validating the interactions. (d) LCA comparing the interaction strength of MaDTX19 (WT), MaDTX19^{SD} (phosphomimetic), and MaDTX19^{SA} (phosphodeficient) with auxin-related proteins. Luminescence intensity reflects interaction strength.

and activating Al^{3+} tolerance through citrate secretion and flavonoid-mediated antioxidant defense. The MaMYB308-mediated negative feedback prevents excessive *MaDTX19* expression, minimizing sustained fitness costs. This two-tier strategy, with rapid phosphorylation for immediate response and transcriptional modulation for long-term optimization, enables mulberry to balance short-term survival with long-term growth. Quantitative analysis of transgenic lines with graded *MaDTX19* expression supports this model. Lines with greater growth suppression showed higher survival rates and lower oxidative damage under Al^{3+} stress. Notably, this relationship plateaued beyond a certain expression threshold, suggesting an optimal MaDTX19 activity level that maximizes tolerance while minimizing fitness costs.

Nevertheless, we acknowledge that our observations across transgenic lines with graded expression levels, while supportive of the adaptive trade-off interpretation, do not constitute definitive proof. Separation-of-function mutants that uncouple Al^{3+} tolerance from growth suppression would provide the strongest genetic evidence for the adaptive nature of this trade-off. Without such evidence, alternative explanations cannot be formally excluded.

https://doi.org/10.48130/forres-0026-0031

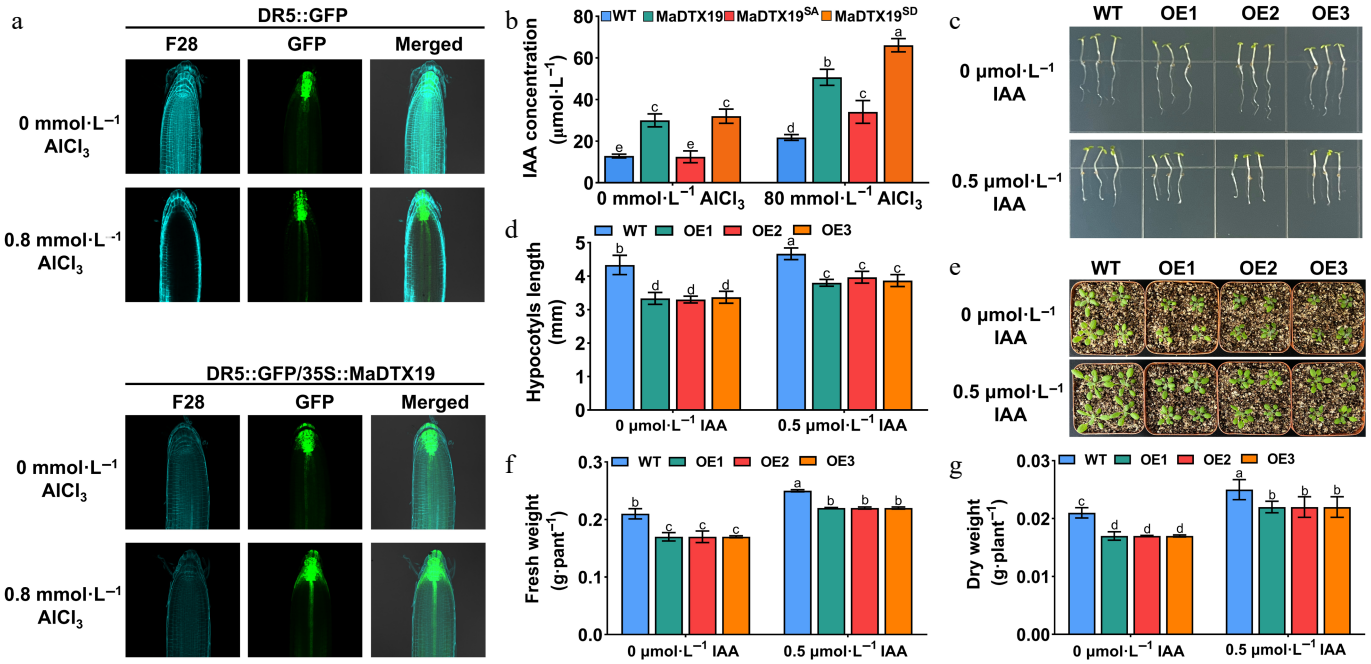


Fig. 11 MaDTX19 modulates auxin homeostasis and spatial distribution in root tips under Al^{3+} stress. (a) DR5::GFP fluorescence imaging of auxin distribution in root tips of WT and *MaDTX19*-OE *Arabidopsis* seedlings under 0 and 0.8 mmol·L^{-1} $AlCl_3$ stress. (b) Quantitative analysis of auxin (IAA) content in root tips of WT and *MaDTX19*-OE seedlings under the same conditions. Effects of exogenous IAA treatment on growth phenotypes of WT and MaDTX19-OE seedlings: (c) hypocotyl phenotype, (d) hypocotyl length, (e) seedling phenotype, (f) fresh weight, and (g) dry weight under standard light conditions. Data are mean ± SD. Different letters indicate significant differences ($p < 0.05$).

Conclusions

Ser4 phosphorylation of MaDTX19 serves as a core regulatory node that synchronously regulates growth inhibition and Al^{3+} tolerance in mulberry. Phosphorylated MaDTX19 modulates auxin homeostasis to restrain plant growth and enhances citrate exudation and antioxidant capacity to confer Al^{3+} tolerance. The MaMYB61-MaMYB308 transcriptional module fine-tunes *MaDTX19* expression to optimize fitness. These findings reveal a post-translational regulatory mechanism of tree adaptation to Al^{3+} stress, and provide promising genetic targets for molecular breeding of Al^{3+}-tolerant mulberry cultivars.

Author contributions

The authors confirm contributions to the paper as follows: study conception and design: Ji X, Gai Y; methodology: Han S, Zhao T, Liu C; validation: Sun M, Han SM; formal analysis: Liu C, Zhao J; investigation: Han S, Zhao T, Zhao J, Wang Y; visualization: Liu Z; draft manuscript preparation: Han S, Zhao T; writing – review & editing: Ji X, Gai Y; supervision: Ji X, Gai Y; project administration: Ji X; funding acquisition: Ji X, Gai Y. All authors reviewed the results and approved the final version of the manuscript.

Data availability

All data generated or analyzed during this study are included in this published article and its supplementary information files.

Acknowledgments

This work was supported by the National Natural Science Foundation of People's Republic of China (Grant Nos 32171748 and 32172799), the Natural Science Foundation of Shandong Province (Grant Nos ZR2024MC211 and ZR2025QC308), and the Modern Agricultural Technology System of Shandong Province (Grant No. SDAIT-18-04).

Conflict of interest

The authors declare that they have no conflict of interest.

Supplementary information accompanies this paper online at: https://doi.org/10.48130/forres-0026-0031.

Dates

Received 13 May 2026; Revised 3 September 2026; Accepted 9 October 2026; Published online 28 October 2026

References

[1] Cope OL, Keefover-Ring K, Kruger EL, Lindroth RL. 2021. Growth-defense trade-offs shape population genetic composition in an iconic forest tree species. *Proceedings of the National Academy of Sciences of the United States of America* 118:e2103162118

[2] He Z, Webster S, He SY. 2022. Growth-defense trade-offs in plants. *Current Biology* 32:R634–R639

[3] Chen ZC, Huang CF. 2024. Sustainable utilization of acid soils. *Plant and Soil* 504:1–3

[4] Munyaneza V, Zhang W, Haider S, Xu F, Wang C, et al. 2024. Strategies for alleviating aluminum toxicity in soils and plants. *Plant and Soil* 504:167–190

[5] Ma Q, Yi R, Li L, Liang Z, Zeng T, et al. 2018. GsMATE encoding a multidrug and toxic compound extrusion transporter enhances aluminum tolerance in *Arabidopsis thaliana*. *BMC Plant Biology* 18:212

[6] Wang H, Ji F, Zhang Y, Hou J, Liu W, et al. 2019. Interactions between hydrogen sulphide and nitric oxide regulate two soybean citrate

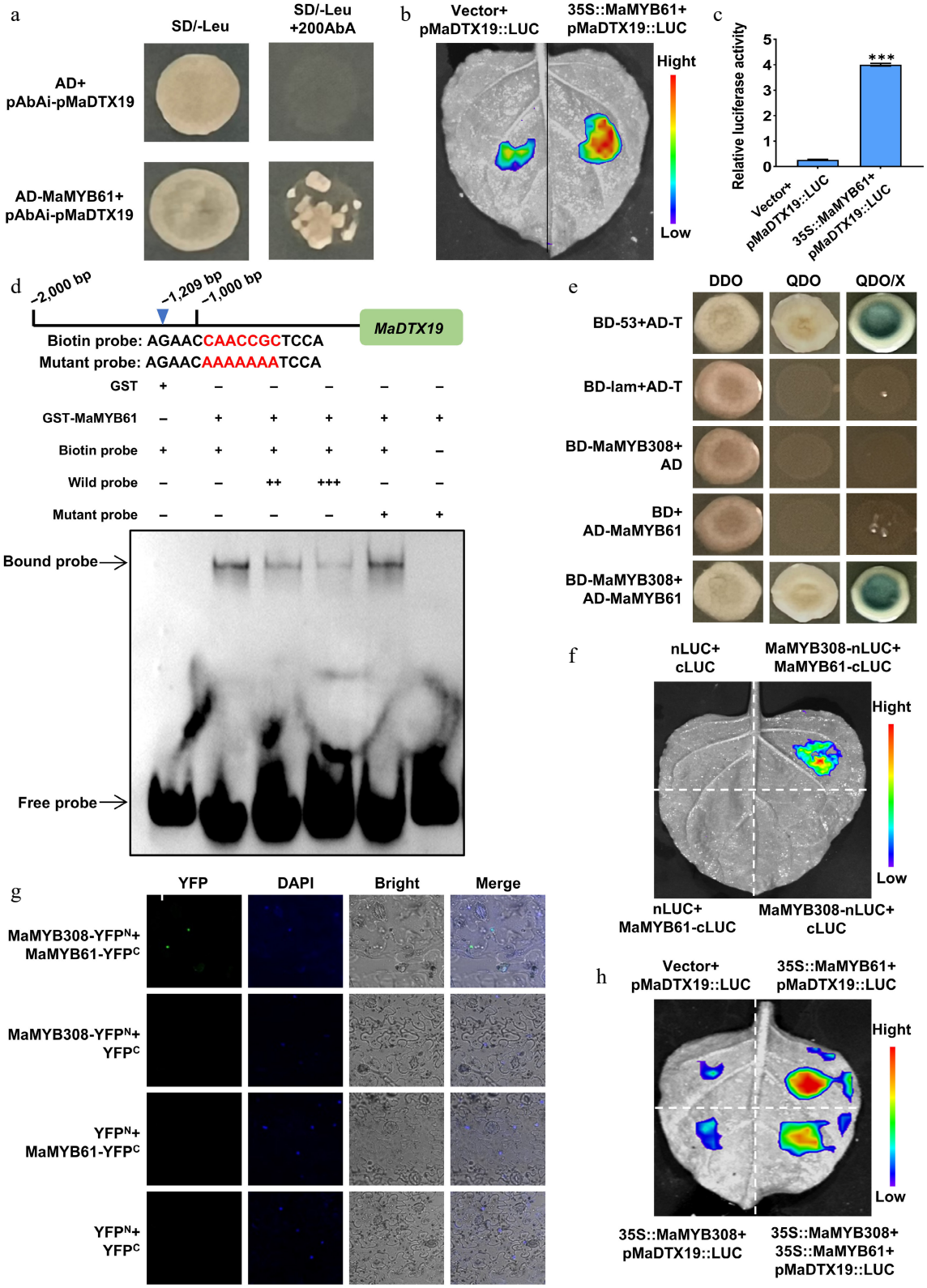


Fig. 12 The MaMYB61/MaMYB308 module fine-tunes *MaDTX19* expression via transcriptional activation and repression. (a) Yeast one-hybrid (Y1H) assay confirming the binding of MaMYB61 to the *MaDTX19* promoter (*pMaDTX19*). Growth on SD/-Leu/AbA medium indicates a positive interaction. (b) Dual-luciferase reporter assay showing that MaMYB61 activates *pMaDTX19* in tobacco leaf epidermal cells. (c) Quantitative analysis of the LUC/REN ratio. (d) EMSA confirming sequence-specific binding of MaMYB61 to the *MaDTX19* promoter. Labeled probes were incubated with recombinant MaMYB61 protein; unlabeled probes were used as competitors. (e) Y2H assay confirming the physical interaction between MaMYB61 and MaMYB308. (f) LCA confirming the physical interaction between MaMYB61 and MaMYB308. (g) BiFC assay localizing the MaMYB61-MaMYB308 interaction to the nucleus. DAPI was used as the nuclear marker. (h) Dual-luciferase reporter assay showing that MaMYB308 attenuates MaMYB61-mediated activation of *pMaDTX19*. All data are mean ± SD of three independent biological replicates. Asterisks indicate significant differences (*t*-test, *** $p < 0.001$).

https://doi.org/10.48130/forres-0026-0031

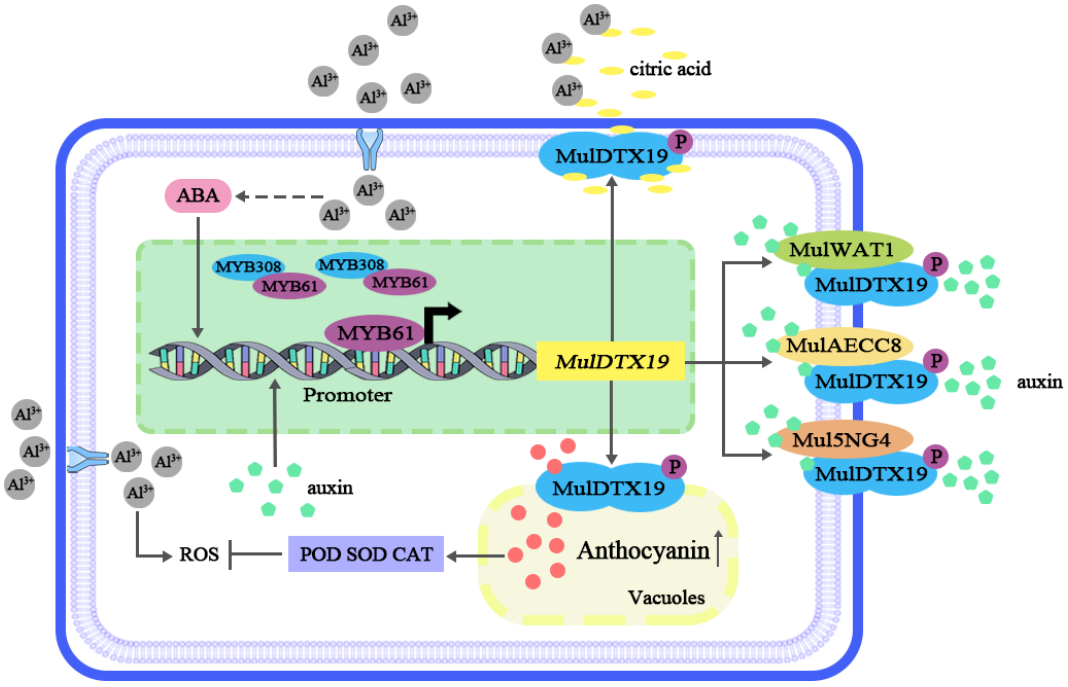


Fig. 13 Hierarchical regulatory model of MaDTX19-mediated growth-defense trade-off in mulberry under Al^{3+} stress. Under optimal conditions, low *MaDTX19* expression and basal Ser4 phosphorylation maintain normal auxin transport and growth. Upon Al^{3+} stress, the MaMYB61-MaMYB308 module induces *MaDTX19* transcription, while a yet-unidentified kinase phosphorylates Ser4, switching MaDTX19 to its active conformation. Phosphorylated MaDTX19 then exerts dual functions: inhibiting growth by interacting with auxin transport components (MaAECC8, Ma5NG4, MaWAT1) and activating Al^{3+} tolerance through citrate secretion and flavonoid-mediated antioxidant defense. The MaMYB308-mediated negative feedback prevents excessive *MaDTX19* expression, minimizing sustained fitness costs.

transporters during the alleviation of aluminium toxicity. *Plant, Cell & Environment* 42:2340–2356

[7] Kar D, Pradhan AA, Datta S. 2021. The role of solute transporters in aluminum toxicity and tolerance. *Physiologia Plantarum* 171:638–652

[8] Magalhães JV, Liu J, Guimarães CT, Lana UGP, Alves VMC, et al. 2007. A gene in the multidrug and toxic compound extrusion (MATE) family confers aluminum tolerance in sorghum. *Nature Genetics* 39:1156–1161

[9] Marinova K, Pourcel L, Weder B, Schwarz M, Barron D, et al. 2007. The *Arabidopsis* MATE transporter TT12 acts as a vacuolar flavonoid/H^+-antiporter active in proanthocyanidin-accumulating cells of the seed coat. *The Plant Cell* 19:2023–2038

[10] Kusakizako T, Miyauchi H, Ishitani R, Nureki O. 2020. Structural biology of the multidrug and toxic compound extrusion superfamily transporters. *Biochimica et Biophysica Acta (BBA) - Biomembranes* 1862:183154

[11] Anfang M, Shani E. 2021. Transport mechanisms of plant hormones. *Current Opinion in Plant Biology* 63:102055

[12] Wang NN, Xiu KY, Deng M, Liu QY, Jin DD, et al. 2024. Effects of phosphorylation on CsTT12 transport function: a comparative phosphoproteomic analysis of flavonoid biosynthesis in tea plants (*Camellia sinensis*). *The Plant Journal* 120:2420–2436

[13] Tripathi A, Singh D, Bhati J, Singh D, Taunk J, et al. 2025. Genome wide identification of MATE and ALMT gene family in lentil (Lens culinaris Medikus) and expression profiling under Al stress condition. *BMC Plant Biology* 25:88

[14] Zhang P, Yu F, Zhu X, Zhao J, Zhang K. 2025. MATE transporter DTX44 is involved in regulating flowering time in *Arabidopsis*. *Physiologia Plantarum* 177:e70238

[15] Zhu K, Ateeq M, Wang X, Huang X, Yang J, et al. 2025. PpMATE49, a multidrug and toxic compound extrusion transporter, confers manganese toxicity tolerance in peach (*Prunus persica*). *Journal of Hazardous Materials* 496:139270

[16] Zhou G, Delhaize E, Zhou M, Ryan PR. 2013. The barley MATE gene, *HvAACT1*, increases citrate efflux and Al^{3+} tolerance when expressed in wheat and barley. *Annals of Botany* 112:603–612

[17] Du H, Ryan PR, Liu C, Li H, Hu W, et al. 2021. ZmMATE6 from maize encodes a citrate transporter that enhances aluminum tolerance in transgenic *Arabidopsis thaliana*. *Plant Science* 311:111016

[18] Gomez C, Terrier N, Torregrosa L, Vialet S, Fournier-Level A, et al. 2009. Grapevine MATE-type proteins act as vacuolar H^+-dependent acylated anthocyanin transporters. *Plant Physiology* 150:402–415

[19] Chen SY, Tang YM, Hu YY, Wang Y, Sun B, et al. 2018. FaTT12-1, a multidrug and toxin extrusion (MATE) member involved in proanthocyanidin transport in strawberry fruits. *Scientia Horticulturae* 231:158–165

[20] Upadhyay N, Kar D, Mahajan BD, Nanda S, Rahiman R, et al. 2019. The multitasking abilities of MATE transporters in plants. *Journal of Experimental Botany* 70:4643–4656

[21] Liu G, Li D, Mai H, Lin X, Lu X, et al. 2024. GmSTOP1-3 regulates flavonoid synthesis to reduce ROS accumulation and enhance aluminum tolerance in soybean. *Journal of Hazardous Materials* 480:136074

[22] Li R, Li J, Li S, Qin G, Novák O, et al. 2014. ADP1 affects plant architecture by regulating local auxin biosynthesis. *PLoS Genetics* 10:e1003954

[23] Wang P, Yu W, Zhang J, Rengel Z, Xu J, et al. 2016. Auxin enhances aluminium-induced citrate exudation through upregulation of GmMATE and activation of the plasma membrane H^+-ATPase in soybean roots. *Annals of Botany* 118:933–940

[24] Bai B, Bian H, Zeng Z, Hou N, Shi B, et al. 2017. miR393-mediated auxin signaling regulation is involved in root elongation inhibition in response to toxic aluminum stress in barley. *Plant and Cell Physiology* 58:426–439

[25] Malangisha GK, Li C, Yang H, Mahmoud A, Ali A, et al. 2021. Permissive action of H_2O_2 mediated *ClUGT75* expression for auxin glycosylation and Al^{3+}-tolerance in watermelon. *Plant Physiology and Biochemistry* 167:77–90

[26] Jiang X, Lai S, Kong D, Hou X, Shi Y, et al. 2023. Al-induced CsUGT84J2 enhances flavonol and auxin accumulation to promote root growth in tea plants. *Horticulture Research* 10:uhad095

[27] Sun P, Tian QY, Chen J, Zhang WH. 2010. Aluminium-induced inhibition of root elongation in *Arabidopsis* is mediated by ethylene and auxin. *Journal of Experimental Botany* 61:347−356

[28] Yang ZB, Geng X, He C, Zhang F, Wang R, et al. 2014. TAA1-regulated local auxin biosynthesis in the root-apex transition zone mediates the aluminum-induced inhibition of root growth in *Arabidopsis*. *The Plant Cell* 26:2889−2904

[29] Liu G, Gao S, Tian H, Wu W, Robert HS, et al. 2016. Local transcriptional control of YUCCA regulates auxin promoted root-growth inhibition in response to aluminium stress in *Arabidopsis*. *PLoS Genetics* 12:e1006360

[30] Daspute AA, Sadhukhan A, Tokizawa M, Kobayashi Y, Panda SK, et al. 2017. Transcriptional regulation of aluminum-tolerance genes in higher plants: clarifying the underlying molecular mechanisms. *Frontiers in Plant Science* 8:1358

[31] Wu X, Li R, Shi J, Wang J, Sun Q, et al. 2014. *Brassica oleracea* MATE encodes a citrate transporter and enhances aluminum tolerance in *Arabidopsis thaliana*. *Plant & Cell Physiology* 55:1426−1436

[32] Zhang H, Zhu H, Pan Y, Yu Y, Luan S, et al. 2014. A DTX/MATE-type transporter facilitates abscisic acid efflux and modulates ABA sensitivity and drought tolerance in *Arabidopsis*. *Molecular Plant* 7:1522−1532

[33] Berry HM, Argueso CT. 2022. More than growth: phytohormone-regulated transcription factors controlling plant immunity, plant development and plant architecture. *Current Opinion in Plant Biology* 70:102309

[34] Gani U, Nautiyal AK, Kundan M, Rout B, Pandey A, et al. 2022. Two homeologous MATE transporter genes, *NtMATE21* and *NtMATE22*, are involved in the modulation of plant growth and flavonol transport in *Nicotiana tabacum*. *Journal of Experimental Botany* 73:6186−6206

[35] Han WH, Zhang FB, Ji SX, Liang KL, Wang JX, et al. 2025. Auxin-salicylic acid seesaw regulates the age-dependent balance between plant growth and herbivore defense. *Science Advances* 11:eadu5141

[36] Wang P, Cao H, Quan S, Wang Y, Li M, et al. 2023. Nitrate improves aluminium resistance through SLAH-mediated citrate exudation from roots. *Plant, Cell & Environment* 46:3518−3541

[37] Fan W, Kong Q, Chen Y, Lu F, Wang S, et al. 2024. Safe utilization and remediation potential of the mulberry-silkworm system in heavy metal-contaminated lands: a review. *Science of the Total Environment* 927:172352

[38] Zhu M, Yang Z, Wang Z, Tsigbey VE, Cui Z, et al. 2025. Mulberry (*Morus alba* L.) planting increased the abundance of soil carbon cycling functional genes by improving soil properties, and further enhanced the stability of soil carbon pool. *Plant and Soil* 515:735−751

[39] Jefferson RA, Kavanagh TA, Bevan MW. 1987. GUS fusions: beta-glucuronidase as a sensitive and versatile gene fusion marker in higher plants. *The EMBO Journal* 6:3901−3907

[40] Su L, Lv A, Wen W, Zhou P, An Y. 2020. Auxin is involved in magnesium-mediated photoprotection in photosystems of alfalfa seedlings under aluminum stress. *Frontiers in Plant Science* 11:746

[41] Bennett C, Sookwong P, Jakmunee J, Mahatheeranont S. 2021. Smartphone digital image colorimetric determination of the total monomeric anthocyanin content in black rice *via* the pH differential method. *Analytical Methods* 13:3348−3358

[42] Doshi R, McGrath AP, Piñeros M, Szewczyk P, Garza DM, et al. 2017. Functional characterization and discovery of modulators of SbMATE, the agronomically important aluminium tolerance transporter from Sorghum bicolor. *Scientific Reports* 7:17996

[43] Li J, Wang R, Li C, Guo X, Li Q, et al. 2026. Posttranslational regulation of TOR kinase activity controls resource allocation between plant growth and immunity in *Arabidopsis*. *Molecular Plant* 19:629−650

[44] Melo JO, Lana UG, Piñeros MA, Alves VM, Guimarães CT, et al. 2013. Incomplete transfer of accessory loci influencing *SbMATE* expression underlies genetic background effects for aluminum tolerance in sorghum. *The Plant Journal* 73:276−288

Copyright: © 2026 by the author(s). Published by Maximum Academic Press, Fayetteville, GA. This article is an open access article distributed under Creative Commons Attribution License (CC BY 4.0), visit https://creativecommons.org/licenses/by/4.0/.